

Time-Domain Multiple Traces Boundary Integral Formulation for Acoustic Wave Scattering in 2D

Carlos Jerez-Hanckes* Ignacio Labarca†

November 17, 2020

Abstract

We present a novel computational scheme to solve acoustic wave transmission problems over composite scatterers, i.e. penetrable obstacles possessing junctions or triple points. Our continuous problem is cast as a multiple traces time-domain boundary integral formulation valid in two and three dimensions. Numerically, our two-dimensional non-conforming spatial discretization uses spectral elements based on second kind Chebyshev polynomials while a convolution quadrature scheme is performed in the complex frequency domain. Computational experiments reveal multistep and multistage convolution quadrature expected convergence results for a variety of complex domains.

Keywords: acoustic wave scattering, wave transmission problems, convolution quadrature, time-domain boundary integral operators, multiple traces formulation

1 Introduction

We are interested in solving acoustic wave transmission problems arising by incident waves propagating through a composite object. More precisely, we consider a bounded Lipschitz domain $\Omega \subset \mathbb{R}^d$, $d = 2, 3$, composed of M non-overlapping Lipschitz subdomains Ω_i , $i = 1, \dots, M$, such that

$$\bar{\Omega} = \bigcup_{\ell=1}^M \bar{\Omega}_\ell, \quad (1)$$

where $\Omega_i \cap \Omega_j = \emptyset$ for $i \neq j$. We call $\Gamma_{ij} := \partial\Omega_i \cap \partial\Omega_j$ the interface between domains Ω_i and Ω_j . We also denote by $\Omega_0 := \mathbb{R}^d \setminus \bar{\Omega}$ the unbounded exterior domain. Notice that one can write

$$\Gamma_i = \partial\Omega_i = \bigcup_{j \in \Upsilon_i} \Gamma_{ij},$$

where Υ_i corresponds to an index set defined by

$$\Upsilon_i := \{j \in \{0, \dots, M\} : j \neq i \text{ and } \Gamma_{ij} \neq \emptyset\}.$$

The above composite material is characterized by piecewise-constant properties, $c_i > 0$ corresponding to the wave-speed on the domain Ω_i , $i = 0, \dots, M$. Assuming some impinging wave,

* (carlos.jerez@uai.cl), Faculty of Engineering and Sciences, Universidad Adolfo Ibáñez, Santiago, Chile

† (ignacio.labarca@sam.math.ethz.ch), Seminar for Applied Mathematics, Swiss Federal Institute of Technology, Zurich, Switzerland

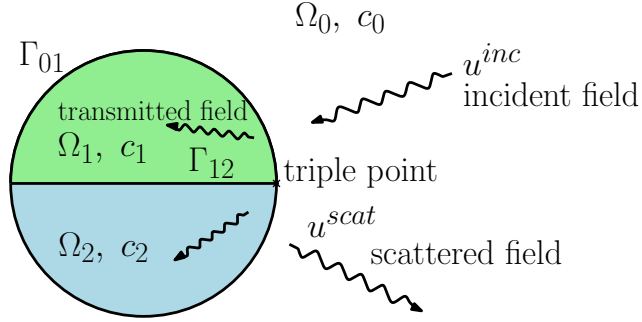


Figure 1: Example of scatterer with two homogenous subdomains.

we denote by $u_i = u|_{\Omega_i}$ the total wave inside Ω_i and by $u_0 = u|_{\Omega_0}$ the scattered wave in the exterior domain. With this, we seek to solve the time-domain acoustic transmission problem:

$$\left\{ \begin{array}{ll} \frac{1}{c_i^2} \frac{\partial^2 u_i}{\partial t^2} - \Delta u_i = 0 & \text{in } \Omega_i \times [0, \infty), \quad i = 0, \dots, M, \\ u_0 - u_j = -u^{\text{inc}} & \text{on } \Gamma_{0j} \times [0, \infty), \quad j \in \Upsilon_0, \\ \frac{\partial u_0}{\partial n^0} + \frac{\partial u_j}{\partial n^j} = -\frac{\partial u^{\text{inc}}}{\partial n^0} & \text{on } \Gamma_{0j} \times [0, \infty), \quad j \in \Upsilon_0, \\ u_i - u_j = 0 & \text{on } \Gamma_{ij} \times (0, \infty], \quad i, j > 0, \quad j \in \Upsilon_i, \\ \frac{\partial u_i}{\partial n^i} + \frac{\partial u_j}{\partial n^j} = 0 & \text{on } \Gamma_{ij} \times [0, \infty), \quad i, j > 0, \quad j \in \Upsilon_i, \\ u_i = \frac{\partial u_i}{\partial t} = 0 & \text{in } \Omega_i \times \{0\}, \quad i = 0, \dots, M. \end{array} \right. \quad (2)$$

We will attempt to solve the above problem by conveniently combining the following ingredients explained below:

- (i) Boundary integral equations (BIEs) in the form of the local multiple traces formulation (MTF);
- (ii) Spectral non-conforming Galerkin with Chebyshev polynomials for spatial discretization of two-dimensional problems; and,
- (iii) Convolution quadrature (CQ) for approximating in the time domain.

When interested in the interior version of the above volume problem, standard methods based on finite differences or finite elements can be used directly. However, for exterior or transmission problems absorbing boundary conditions must be enforced, usually done via perfectly matched layers [9]. Alternatively, BIEs avoid this difficulty given that fundamental solutions rigorously capture the radiation conditions of the problem. Hence, instead of solving partial differential

equations one solves BIEs, whose unknowns are densities defined on boundaries and which may have physical meaning or not, depending whether direct or indirect formulations are employed.

For time-harmonic wave scattering over composite materials, one can resort to BIEs based on single-trace or local and global versions of MTFs (*cf.* [23, 10, 11]), respectively based on the strong or weak enforcement of transmission conditions. These lead to well-posed problems in such complex materials. The discretization of such MTF-BIEs then may be formulated by the boundary element method (BEM) [23], spectral Galerkin [25, 26] or Nyström [24] methods. We chose a spectral variational scheme for the local MTF based on Chebyshev polynomials for the discretization of two-dimensional problems in order to have a high-order solution with a small number of degrees of freedom. Also, in this setting matrix entries can efficiently be computed via the Fast Fourier Transform (FFT) by relating Chebyshev coefficients with Fourier coefficients [25, Section 3.3][38, Chapter 3]. The use of built-in preconditioners based on the Calderon operator make the local MTF attractive in contrast of other first kind BIEs for composite materials [25]. A good alternative could be the second kind single-trace formulation [12], but the analysis of second kind integral equations in time-domain is not clear [36, Section 1.6]. Numerical analysis of the discrete problem in the time domain remains open, in particular because existing results based on semigroups of linear operators [32] already used for transmission problems (*cf.* [34, 35]) requires Galerkin discretization in standard Sobolev spaces.

Still, we need to solve time-domain wave propagation problems, and thus we opt to use CQ methods [8]. Lately, CQ schemes have attracted much attention due to their stability and possibility to implement as a blackbox with complex frequency-domain solvers. In particular, we employ the local MTF as it allows easy parallelization and fast solvers, such as [25, 26]. Many theoretical aspects of the CQ method along with numerical analysis results are given in the monograph [36]. Algorithmically, we refer to [19] for the corresponding pseudo-code to efficiently compute forward convolutions and solve convolution equations. A thorough analysis of multistage CQ can be found in [3, 4, 6, 31], while generalized CQ allowing for different timesteps is described in [27, 28]. The implementation and analysis of the method in the context of scattering problems has been studied in [7], for transmission problems in [33, 34], and composite materials with a first kind single-trace formulation in [35] and [17]. Fast multipole method for three dimensional scattering using CQ is studied in [2]. Yet, to our knowledge, no time-domain CQ MTF has been described in the literature. In fact, only semi-implicit time schemes have been coupled to local MTF to describe non-linear dynamics of neural transmission [22, 21].

Direct Galerkin for space-time BIEs could also be used to tackle Problem (2), but this involves the difficult computation of boundary integral operators in time domain [8]. Moreover, as it happens in most of timestepping procedures, a bad choice of the timestep Δt may lead to instabilities. Also, long-time computations frequently produce stability problems. Although there are remedies to deal with these difficulties [13, 14, 15, 16] as well as other stable formulations in time-domain [1], CQ remains a simple, efficient and stable method to discretize time domain problems without major complications.

In what follows, we set the framework required to apply CQ to solve the time-domain acoustic transmission problem (2) in composite materials via the local MTF [23, 25, 26]. In Section 2, we present the MTF in frequency domain as described in [23]. Section 3 recalls the main ideas behind time-domain BIEs. Section 4 describes our numerical scheme including the spectral non-conforming Galerkin discretization for MTF [25, 26]. Then, in Sections 5, 5.1 and 5.2 we explain CQ for multistep and multistage linear methods and the corresponding application for the Petrov-Galerkin formulation with spectral elements as convolutional equations in Section 5.3. Finally, in Section 6 we show some numerical experiments for different geometries and parameters of interest, which clearly illustrate the capabilities of the proposed methodology and set future research ideas.

Notation used throughout the article is briefly explained here:

- u denotes a field in the space and time domain, related to the acoustic wave equation (see (2)).
- U and V denote fields in the frequency domain, related to the modified Helmholtz equation (see Section 2).
- λ, φ, ψ denote densities in the time domain, with values in Sobolev spaces defined over a boundary $\partial\Omega$ or an interface Γ_{ij} (see Section 3, (27) and Problem 3.2)
- Λ, Φ, Ψ are densities in the frequency domain (see Section 2, (3), (10)).
- Bold variables $\boldsymbol{\lambda}, \boldsymbol{\varphi}, \boldsymbol{g}, \boldsymbol{\Lambda}, \boldsymbol{\Phi}, \boldsymbol{G}$ denote elements of product spaces (see Problems 2.3, 3.2, 4.1, 5.1 and 5.3).
- Operators $A, C, S, D, K, K', V, W, X, E, R, L$ are defined in the frequency domain, sometimes depending on a complex parameter $s \in \mathbb{C}_+$ (see Section 2, (10), (12), (13), (14)).
- Operators $\mathcal{A}, \mathcal{C}, \mathcal{S}, \mathcal{D}, \mathcal{K}, \mathcal{K}', \mathcal{V}, \mathcal{W}, \mathcal{F}$ are defined in the time domain by means of the inverse Laplace transform over frequency domain counterparts (see Section 3, (27), (28), (29) and Problem 3.2).
- M is the number of subdomains (see (1)).
- N is the number of timesteps (see Problem 5.1).
- L refers to the dimension of the spectral spatial discretization (see Section 4.1, Problem (4.1)).
- Variable $s \in \mathbb{C}_+$ is reserved for the parameter in Laplace domain and modified Helmholtz equations (see Section 2, (9), (10), (11), (12)).
- Variables $c_j \in \mathbb{R}$ are the wavespeed in domains Ω_j , $j = 0, 1, 2, \dots$ (see (2)).
- The polynomial $\delta(\zeta)$ determines a multistep method (see Section 5.1, (44)).
- The matrix $\delta^{\text{RK}}(\zeta)$ determines a multistage method (see Section 5.2, (50)).

2 Multiple traces formulation

We recall notation and results for the local MTF for the Helmholtz equation as exposed in [23, 26]. Let $\Omega \subset \mathbb{R}^2$ be a bounded Lipschitz domain composed of M non-overlapping Lipschitz subdomains $\Omega_\ell, \ell = 1, \dots, M$, such that

$$\overline{\Omega} = \bigcup_{\ell=1}^M \overline{\Omega}_\ell,$$

where $\Omega_i \cap \Omega_j = \emptyset$ for $i \neq j$. Let \boldsymbol{n}^i be the unit outward normal vector to $\partial\Omega_i$. Standard Sobolev spaces of order $s \in \mathbb{R}$ in Ω_i are written $H^s(\Omega_i)$, $H^s(\partial\Omega_i)$ on the boundary. For an open interface $\Gamma_{ij} := \partial\Omega_i \cap \partial\Omega_j$ and $s > 0$, we denote

$$H^s(\Gamma_{ij}) := \{\xi|_{\Gamma_{ij}} : \xi \in H^s(\partial\Omega_i)\}$$

and

$$\tilde{H}^s(\Gamma_{ij}) := \{\eta \in H^s(\Gamma_{ij}) : \tilde{\eta} \in H^s(\partial\Omega_i)\},$$

where $\tilde{\eta}$ is the extension by zero of η over $\partial\Omega_i$. For negative values $s < 0$, we identify $\tilde{H}^s(\Gamma_{ij})$ with the dual space of $H^{-s}(\Gamma_{ij})$. Product trace spaces over closed boundaries $\partial\Omega_\ell$ are denoted

$$\mathbf{V}_\ell^s := H^{s+\frac{1}{2}}(\partial\Omega_\ell) \times H^{s-\frac{1}{2}}(\partial\Omega_\ell), \quad s \in \mathbb{R},$$

equipped with the norm $\|\cdot\|_{\mathbf{V}_\ell^s} = \|\cdot\|_{H^{s+\frac{1}{2}}(\partial\Omega_\ell)} + \|\cdot\|_{H^{s-\frac{1}{2}}(\partial\Omega_\ell)}$, and set $\mathbf{V}_\ell \equiv \mathbf{V}_\ell^0$. Moreover, we use the sesquilinear duality product:

$$(\Lambda, \Phi)_{\times, \ell} = \langle \Lambda_d, \overline{\Phi}_n \rangle_{\Gamma_\ell} + \langle \overline{\Phi}_d, \Lambda_n \rangle_{\Gamma_\ell} \quad (3)$$

for $\Lambda, \Phi \in \mathbf{V}_\ell$, $\Lambda = (\Lambda_d, \Lambda_n)$, and $\Phi = (\Phi_d, \Phi_n)$. For the multiple interfaces case we need piecewise or broken spaces:

$$\tilde{H}_{\text{pw}}^{\mp\frac{1}{2}}(\partial\Omega_i) := \left\{ V \in H^{\mp\frac{1}{2}}(\partial\Omega_i) : V|_{\Gamma_{ij}} \in \tilde{H}^{\mp\frac{1}{2}}(\Gamma_{ij}), \quad \forall j \in \Upsilon_i \right\}, \quad (4)$$

whose duals are

$$H_{\text{pw}}^{\pm\frac{1}{2}}(\partial\Omega_i) := \left\{ V \in \mathcal{D}'(\partial\Omega_i) : V|_{\Gamma_{ij}} \in H^{\pm\frac{1}{2}}(\Gamma_{ij}), \quad \forall j \in \Upsilon_i \right\}. \quad (5)$$

With (4) and (5) we define the Cartesian product spaces:

$$\begin{aligned} \mathbf{V}_{\text{pw},i} &:= H_{\text{pw}}^{\frac{1}{2}}(\partial\Omega_i) \times H_{\text{pw}}^{-\frac{1}{2}}(\partial\Omega_i), \\ \tilde{\mathbf{V}}_i &:= H^{\frac{1}{2}}(\partial\Omega_i) \times \tilde{H}_{\text{pw}}^{-\frac{1}{2}}(\partial\Omega_i), \\ \tilde{\tilde{\mathbf{V}}}_i &:= \tilde{H}_{\text{pw}}^{\frac{1}{2}}(\partial\Omega_i) \times \tilde{H}_{\text{pw}}^{-\frac{1}{2}}(\partial\Omega_i). \end{aligned}$$

We will also need the space $\tilde{\mathbf{V}}_{ij} := H^{\frac{1}{2}}(\Gamma_{ij}) \times \tilde{H}^{-\frac{1}{2}}(\Gamma_{ij})$, along with MTF spaces defined over $M \in \mathbb{N}$ subdomain boundaries:

$$\begin{aligned} \tilde{\tilde{\mathbf{V}}}_M &:= \tilde{\tilde{\mathbf{V}}}_0 \times \dots \times \tilde{\tilde{\mathbf{V}}}_M \\ \tilde{\mathbf{V}}_M &:= \tilde{\mathbf{V}}_0 \times \dots \times \tilde{\mathbf{V}}_M \\ \mathbf{V}_M &:= \mathbf{V}_0 \times \dots \times \mathbf{V}_M \\ \mathbf{V}_{\text{pw},M} &:= \mathbf{V}_{\text{pw},0} \times \dots \times \mathbf{V}_{\text{pw},M} \end{aligned}$$

We denote by γ_d^i and γ_n^i the standard Dirichlet and Neumann trace operators taken from the interior of Ω_i and set the vector trace operator $\gamma^i V := (\gamma_d^i V, \gamma_n^i V) : H_{\text{loc}}^1(\Delta, \Omega_i) \rightarrow \mathbf{V}_i$, where

$$H_{\text{loc}}^1(\Delta, \Omega_i) := \{V \in H_{\text{loc}}^1(\Omega_i) : \Delta V \in L^2(\Omega_i)\}.$$

Let Ω_i^c be the complement of Ω_i . We now consider traces taken from the exterior, which are denoted $\gamma_d^{i,c}$, $\gamma_n^{i,c}$ and $\gamma^{i,c}$ respectively. Neumann traces $\gamma_n^{i,c}$ involve the unit normal pointing toward the interior of Ω_i^c . Assume that Ω_j and Ω_i^c share an interface Γ_{ij} , then the following transmission conditions hold

$$\gamma_d^j V|_{\Gamma_{ij}} = \gamma_d^{i,c} V|_{\Gamma_{ij}} \quad \text{and} \quad \gamma_n^j V|_{\Gamma_{ij}} = -\gamma_n^{i,c} V|_{\Gamma_{ij}}$$

due to the opposite normal vectors \mathbf{n}^i and \mathbf{n}^j in the interface. Using the operator

$$X_i := \begin{pmatrix} \text{Id}_i & 0 \\ 0 & -\text{Id}_i \end{pmatrix} : \mathbf{V}_i \rightarrow \mathbf{V}_i,$$

we can rewrite transmission conditions as

$$\gamma^{i,c}V|_{\Gamma_{ij}} = (X_j\gamma^j)V|_{\Gamma_{ij}}. \quad (6)$$

We define average and jump trace operators over $\partial\Omega_i$:

$$\llbracket \gamma V \rrbracket_i := \begin{pmatrix} \llbracket \gamma_d V \rrbracket_i \\ \llbracket \gamma_n V \rrbracket_i \end{pmatrix} = \begin{pmatrix} \gamma_d^{i,c}V - \gamma_d^i V \\ \gamma_n^{i,c}V - \gamma_n^i V \end{pmatrix} \quad \text{and} \quad \{\!\!\{ \gamma V \}\!\!\}_i := \begin{pmatrix} \{\!\!\{ \gamma_d V \}\!\!\}_i \\ \{\!\!\{ \gamma_n V \}\!\!\}_i \end{pmatrix} = \frac{1}{2} \begin{pmatrix} \gamma_d^{i,c}V + \gamma_d^i V \\ \gamma_n^{i,c}V + \gamma_n^i V \end{pmatrix}, \quad (7)$$

For the latter, the action at the interface Γ_{ij} is equivalent to

$$\{\!\!\{ \gamma V \}\!\!\}_{ij} = \frac{1}{2}(X_j\gamma^jV + \gamma^iV)|_{\Gamma_{ij}}. \quad (8)$$

Let $G_\ell(|\mathbf{x} - \mathbf{y}|; s) = \frac{i}{4}H_0^{(1)}(is_\ell|\mathbf{x} - \mathbf{y}|)$ denote the fundamental solution of the homogenous equation

$$-\Delta U + s_\ell^2 U = 0 \quad \text{in } \mathbb{R}^d \setminus \partial\Omega_\ell, \quad (9)$$

where $s_\ell = sc_\ell^{-1}$, $s \in \mathbb{C}_+ := \{s \in \mathbb{C} : \text{Re}(s) > 0\}$, $i = \sqrt{-1}$ and $H_0^{(1)}(\cdot)$ denotes the first kind Hankel function of order zero. We define layer potentials acting on sufficiently smooth densities Ψ and Φ on a boundary $\Gamma_\ell = \partial\Omega_\ell$ as

$$\begin{aligned} (\mathbf{S}_\ell(s)\Psi)(\mathbf{x}) &:= \int_{\Gamma_\ell} G_\ell(|\mathbf{x} - \mathbf{y}|; s)\Psi(\mathbf{y})ds_y, \\ (\mathbf{D}_\ell(s)\Phi)(\mathbf{x}) &:= \int_{\Gamma_\ell} \mathbf{n}^\ell(\mathbf{y}) \cdot \nabla_{\mathbf{y}} G_\ell(|\mathbf{x} - \mathbf{y}|; s)\Phi(\mathbf{y})ds_y. \end{aligned} \quad (10)$$

The integral representation formula for a solution U of (9) in $\mathbb{R}^2 \setminus \partial\Omega_\ell$ yields

$$U(\mathbf{x}) = (\mathbf{D}_\ell(s)\llbracket \gamma_d U \rrbracket_\ell)(\mathbf{x}) - (\mathbf{S}_\ell(s)\llbracket \gamma_n U \rrbracket_\ell)(\mathbf{x}), \quad \mathbf{x} \in \mathbb{R}^2 \setminus \partial\Omega_\ell. \quad (11)$$

For each subdomain Ω_ℓ , we introduce corresponding boundary integral operators (BIOs):

$$\begin{aligned} \mathbf{V}_\ell(s) &:= \{\!\!\{ \gamma_d \mathbf{S}_\ell(s) \}\!\!\}_\ell : H^{-\frac{1}{2}}(\partial\Omega_\ell) \rightarrow H^{\frac{1}{2}}(\partial\Omega_\ell), \\ \mathbf{K}'_\ell(s) &:= \{\!\!\{ \gamma_n \mathbf{S}_\ell(s) \}\!\!\}_\ell : H^{-\frac{1}{2}}(\partial\Omega_\ell) \rightarrow H^{-\frac{1}{2}}(\partial\Omega_\ell), \\ \mathbf{K}_\ell(s) &:= \{\!\!\{ \gamma_d \mathbf{D}_\ell(s) \}\!\!\}_\ell : H^{\frac{1}{2}}(\partial\Omega_\ell) \rightarrow H^{\frac{1}{2}}(\partial\Omega_\ell), \\ \mathbf{W}_\ell(s) &:= -\{\!\!\{ \gamma_n \mathbf{D}_\ell(s) \}\!\!\}_\ell : H^{\frac{1}{2}}(\partial\Omega_\ell) \rightarrow H^{-\frac{1}{2}}(\partial\Omega_\ell). \end{aligned} \quad (12)$$

By taking interior and exterior traces to (11) one obtains the formulas for Calderón projectors. These are derived from the definition of BIOs (12) and the continuity properties of single and double layer potentials (10). Interior and exterior Calderón projectors then correspond to

$$\mathbf{C}_\ell(s) := \frac{1}{2}\text{Id} + \mathbf{A}_\ell(s) \quad \text{and} \quad \mathbf{C}_\ell^c(s) := \frac{1}{2}\text{Id} - \mathbf{A}_\ell(s), \quad (13)$$

where

$$\mathbf{A}_\ell(s) := \begin{pmatrix} -\mathbf{K}_\ell(s) & \mathbf{V}_\ell(s) \\ \mathbf{W}_\ell(s) & \mathbf{K}'_\ell(s) \end{pmatrix} : \mathbf{V}_\ell \rightarrow \mathbf{V}_\ell. \quad (14)$$

The following lemma corresponds to an ellipticity property for the Calderón operator (14). It is a slight modification of [5, Lemma 3.1] (scaling of integral operators is not used). Note that indices corresponding to subdomains will be dropped for the sake of brevity.

Lemma 2.1. *Let $\Omega \subset \mathbb{R}^2$ be a bounded Lipschitz domain with boundary Γ . There exists a constant $\beta > 0$ depending on the domain Ω such that the Calderón operator (14) satisfies*

$$\operatorname{Re} \left\{ \left(A(s) \begin{pmatrix} \Phi \\ \Psi \end{pmatrix}, \begin{pmatrix} \Phi \\ \Psi \end{pmatrix} \right)_{\times} \right\} \geq \beta \min(|s|^{-2}, |s|^2) \min(1, |s|^2) \frac{\operatorname{Re}(s)}{|s|^2} \left(\|\Phi\|_{H^{\frac{1}{2}}(\Gamma)}^2 + \|\Psi\|_{H^{-\frac{1}{2}}(\Gamma)}^2 \right) \quad (15)$$

for $\operatorname{Re}(s) > 0$ and for all $\Phi \in H^{\frac{1}{2}}(\Gamma)$ and $\Psi \in H^{-\frac{1}{2}}(\Gamma)$.

Remark 2.2. *Explicit bounds with respect to the complex parameter s will be used in Section 3. In general, ellipticity constants are related to continuity ones of the inverse operators, relevant to properly define their time domain counterparts.*

Transmission conditions at interfaces Γ_{ij} require extension-by-zero and restriction of traces defined over an entire subdomain boundary $\partial\Omega_i$. For this, we define the following operators:

$$\text{restriction: } \mathbf{R}_{ij}^D : H_{\text{pw}}^{\frac{1}{2}}(\partial\Omega_i) \rightarrow H^{\frac{1}{2}}(\Gamma_{ij}), \quad (16)$$

$$\text{extend by zero: } \mathbf{E}_{ij}^D : H^{\frac{1}{2}}(\Gamma_{ij}) \rightarrow H_{\text{pw}}^{\frac{1}{2}}(\partial\Omega_i), \quad (17)$$

and their dual adjoints, denoted by

$$\mathbf{E}_{ij}^N := (\mathbf{R}_{ij}^D)' : \tilde{H}^{-\frac{1}{2}}(\Gamma_{ij}) \rightarrow \tilde{H}_{\text{pw}}^{-\frac{1}{2}}(\partial\Omega_i), \quad (18)$$

$$\mathbf{R}_{ij}^N := (\mathbf{E}_{ij}^D)' : \tilde{H}_{\text{pw}}^{-\frac{1}{2}}(\partial\Omega_i) \rightarrow \tilde{H}^{-\frac{1}{2}}(\Gamma_{ij}). \quad (19)$$

Let us now define the restriction operator over Γ_{ij} :

$$\mathbf{R}_{ij} : H_{\text{pw}}^{\frac{1}{2}}(\partial\Omega_i) \times \tilde{H}_{\text{pw}}^{-\frac{1}{2}}(\partial\Omega_i) \rightarrow \tilde{\mathbf{V}}_{ij} \text{ as } \mathbf{R}_{ij} := \begin{cases} \begin{pmatrix} \mathbf{R}_{ij}^D & 0 \\ 0 & \mathbf{R}_{ij}^N \end{pmatrix} & \text{if } j \in \Upsilon_i, \\ \mathbf{0} & \text{any other case,} \end{cases} \quad (20)$$

for all $j \in \{0, \dots, N\}$. Its dual operator is

$$\mathbf{R}'_{ij} : \tilde{\mathbf{V}}'_{ij} \rightarrow \tilde{H}_{\text{pw}}^{-\frac{1}{2}}(\partial\Omega_i) \times H_{\text{pw}}^{\frac{1}{2}}(\partial\Omega_i) \text{ as } \mathbf{R}'_{ij} := \begin{cases} \begin{pmatrix} \mathbf{E}_{ij}^N & 0 \\ 0 & \mathbf{E}_{ij}^D \end{pmatrix} & \text{if } j \in \Upsilon_i, \\ \mathbf{0} & \text{any other case,} \end{cases} \quad (21)$$

for all $j \in \{0, \dots, N\}$. We will also denote \mathbf{R}_{ij}^\dagger the adjoint operator with respect to $(\cdot, \cdot)_{\times, i}$. These operators let us define

$$\tilde{\mathbf{X}}_{ji} = \mathbf{R}_{ji}^\dagger \mathbf{R}_{ij} \mathbf{X}_i : \mathbf{V}_i \rightarrow \mathbf{V}_{\text{pw}, j} \quad (\text{or } \tilde{\mathbf{V}}_i \rightarrow \tilde{\mathbf{V}}_j), \quad (22)$$

which is used to enforce transmission conditions over the interfaces Γ_{ij} [23].

For $\mathbf{\Lambda} = (\Lambda_0, \dots, \Lambda_M) \in \mathbb{V}_M$, $\mathbf{\Phi} = (\Phi_0, \dots, \Phi_M) \in \tilde{\mathbb{V}}_M$ we denote $(\mathbf{\Lambda}, \mathbf{\Phi})_{\times} = \sum_{\ell=0}^M (\Lambda_\ell, \Phi_\ell)_{\times, \ell}$.

Now, we are able to present the complex frequency-domain MTF:

Problem 2.3 (Multiple traces formulation). *Seek $\mathbf{\Lambda} \in \mathbb{V}_M$ such that the variational form:*

$$(\mathbf{F}(s)\mathbf{\Lambda}, \mathbf{\Phi})_{\times} = (\mathbf{G}, \mathbf{\Phi})_{\times}, \quad \text{for all } \mathbf{\Phi} \in \tilde{\mathbb{V}}_M, \quad (23)$$

is satisfied for $\mathbf{G} = (G_0, G_1, \dots, G_M) \in \mathbb{V}_{pw, M}$ with

$$\mathbf{F}(s) := \begin{pmatrix} \mathbf{A}_0(s) & -\frac{1}{2}\tilde{\mathbf{X}}_{01} & \dots & -\frac{1}{2}\tilde{\mathbf{X}}_{0N} \\ -\frac{1}{2}\tilde{\mathbf{X}}_{10} & \mathbf{A}_1(s) & \dots & -\frac{1}{2}\tilde{\mathbf{X}}_{1N} \\ \vdots & \vdots & \ddots & \vdots \\ -\frac{1}{2}\tilde{\mathbf{X}}_{N0} & -\frac{1}{2}\tilde{\mathbf{X}}_{N1} & \dots & \mathbf{A}_M(s) \end{pmatrix} : \mathbb{V}_M \rightarrow \mathbb{V}_{M, pw}. \quad (24)$$

Remark 2.4. For the case of an incident field U^{inc} coming from Ω_0 , the right-hand side can be described explicitly by

$$\mathbf{G} = \frac{1}{2} \begin{pmatrix} X_0 \gamma_0 U^{inc} \\ -\mathbf{R}_{10}^\dagger \mathbf{R}_{01} \gamma_0 U^{inc} \\ \vdots \\ -\mathbf{R}_{M0}^\dagger \mathbf{R}_{0M} \gamma_0 U^{inc} \end{pmatrix}.$$

Lemma 2.5. The multiple traces operator $\mathbf{F}(s)$ is \mathbb{V}_M -elliptic for $\mathbf{\Lambda} \in \tilde{\mathbb{V}}_M$, i.e. there exists a constant $\beta > 0$ such that

$$\operatorname{Re} \{ (\mathbf{F}(s)\mathbf{\Lambda}, \mathbf{\Lambda})_\times \} \geq \beta \min_{\ell=0, \dots, M} \left\{ \min(|s_\ell|^{-2}, |s_\ell|^2) \min(1, |s_\ell|^2) \frac{\operatorname{Re}(s_\ell)}{|s_\ell|^2} \right\} \|\mathbf{\Lambda}\|_{\mathbb{V}_M}^2, \quad (25)$$

for all $\mathbf{\Lambda} \in \tilde{\mathbb{V}}_M$, where $s_\ell = sc_\ell^{-1}$, $s \in \mathbb{C}_+$. This result also holds for $\mathbf{\Lambda} \in \tilde{\tilde{\mathbb{V}}}_M \subset \tilde{\mathbb{V}}_M$.

It is easy to show the well-posedness of Problem 2.3 from the corresponding result of its real wavenumber counterpart (Helmholtz transmission problem) studied in [23].

Theorem 2.6 (Existence and Uniqueness). *There exists a unique solution to Problem 2.3.*

Proof. The bilinear form induced by $\mathbf{F}(s)$ is continuous in $\mathbb{V}_M \times \tilde{\tilde{\mathbb{V}}}_M$ as in the case of the Helmholtz transmission problem with real wavenumbers [23, Theorem 8]. By Lemma 2.5 we obtain \mathbb{V}_M -ellipticity of $\mathbf{F}(s)$ in the spaces $\tilde{\mathbb{V}}_M$ (or $\tilde{\tilde{\mathbb{V}}}_M \subseteq \tilde{\mathbb{V}}_M$). Existence follows by Lion's projection lemma for the variational formulation in $\mathbb{V}_M \times \tilde{\tilde{\mathbb{V}}}_M$, whereas uniqueness is retrieved by the density of $\tilde{\tilde{\mathbb{V}}}_M$ in \mathbb{V}_M [25, Proposition 2] [23, Remark 11]. \square

As in the real wavenumber Helmholtz case, one can request more regularity to perform a symmetric variational formulation in $\tilde{\mathbb{V}}_M \times \tilde{\mathbb{V}}_M$. The bilinear form remains bounded in these spaces [23, Theorem 8] and the Lax-Milgram theorem leads to existence and uniqueness.

3 Time Domain BIEs

In this section, we shift our attention to a time-domain formulation based on the operator $\mathbf{F}(s)$ and the Laplace transform following [36].

Let us recall the Laplace transform and its inverse for a function $f \in L^2(\mathbb{R}_+)$

$$F(s) := (\mathcal{L}f)(s) := \int_0^\infty f(t)e^{-st}dt, \quad f(t) = (\mathcal{L}^{-1}F(s))(t) := \frac{1}{2\pi i} \int_{\sigma-i\infty}^{\sigma+i\infty} e^{st}F(s)ds, \quad (26)$$

where $\sigma > 0$. These definitions can be easily extended to vector-valued causal distributions [19, Section 1.2] [36, Section 2.1]. For density functions $\psi : \mathbb{R}_+ \rightarrow H^{-\frac{1}{2}}(\Gamma)$ and $\varphi : \mathbb{R}_+ \rightarrow H^{\frac{1}{2}}(\Gamma)$

that can be extended to causal tempered distributions with values in Sobolev spaces and their corresponding Laplace transforms $\Psi : \mathbb{C}_+ \rightarrow H^{-\frac{1}{2}}(\Gamma)$ and $\Phi : \mathbb{C}_+ \rightarrow H^{\frac{1}{2}}(\Gamma)$, we define time-domain single and double layer potentials as

$$\mathcal{S} * \psi := \mathcal{L}^{-1}(\mathcal{S}(s)\Psi(s)), \quad \mathcal{D} * \varphi := \mathcal{L}^{-1}(\mathcal{D}(s)\Phi(s)), \quad (27)$$

where $\mathcal{S}(s)$ and $\mathcal{D}(s)$ are the single and double layer potentials for the (modified) Helmholtz equation $-\Delta U + s^2 U = 0$ defined in (10). In general, having a transfer function $F(s) : X \rightarrow Y$ in the Laplace domain, we will define the corresponding convolutional operator in time domain as

$$\mathcal{F} * \varphi := \mathcal{L}^{-1}(F(s)\Phi(s)), \quad (28)$$

with $(\mathcal{L}\varphi)(s) = \Phi(s)$ and $\Phi(s) \in X$ for all $s \in \mathbb{C}_+$. Details about the existence of this operator can be found in [36, Propositions 3.1.1 and 3.1.2]. Then, we are able to define Calderón BIOs in the time domain by means of the inverse Laplace transform and corresponding operators for the modified Helmholtz equation.

Remark 3.1. *It is common to find the notation of operational calculus $F(\partial_t)\varphi = \mathcal{F} * \varphi$ to emphasize the fact that convolutional operators \mathcal{F} are defined by their Laplace domain counterparts F .*

We define the time-domain Calderón operator:

$$\mathcal{A} := \begin{pmatrix} -\mathcal{K} & \mathcal{V} \\ \mathcal{W} & \mathcal{K}' \end{pmatrix} \quad (29)$$

with \mathcal{V} , \mathcal{K} , \mathcal{K}' and \mathcal{W} being the time-domain single layer, double layer, adjoint-double layer and hypersingular BIOs based on (12) and (28). We can finally write a time-domain version of MTF.

Problem 3.2. *We seek a causal \mathbb{V}_M -valued distribution λ such that*

$$\mathcal{F} * \lambda = \mathbf{g}, \quad (30)$$

where

$$\mathcal{F} := \begin{pmatrix} \mathcal{A}_0 & -\frac{1}{2}\tilde{\mathcal{X}}_{01} \otimes \delta_0 & \dots & -\frac{1}{2}\tilde{\mathcal{X}}_{0N} \otimes \delta_0 \\ -\frac{1}{2}\tilde{\mathcal{X}}_{10} \otimes \delta_0 & \mathcal{A}_1 & \dots & -\frac{1}{2}\tilde{\mathcal{X}}_{1N} \otimes \delta_0 \\ \vdots & \vdots & \ddots & \vdots \\ -\frac{1}{2}\tilde{\mathcal{X}}_{N0} \otimes \delta_0 & -\frac{1}{2}\tilde{\mathcal{X}}_{N1} \otimes \delta_0 & \dots & \mathcal{A}_M \end{pmatrix} \quad \text{and} \quad \mathbf{g} = \frac{1}{2} \begin{pmatrix} X_0 \gamma_0 u^{inc} \\ -\mathbf{R}_{10}^\dagger \mathbf{R}_{01} \gamma_0 u^{inc} \\ \vdots \\ -\mathbf{R}_{M0}^\dagger \mathbf{R}_{0M} \gamma_0 u^{inc} \end{pmatrix} \quad (31)$$

with \mathbf{g} in the Bochner space $C^1([0, \infty); \mathbb{V}_{pw, M})$.

4 Spectral non-conforming Galerkin discretization

We now describe the numerical scheme proposed to solve Problem 3.2. First, we introduce a spectral non-conforming Galerkin discretization of Problem 2.3 based on Chebyshev polynomials of the second kind, originally presented in [25, 26]. Indeed, this alternative yields high-order error convergence rates as confirmed by our numerical experiments in Section 6.1. Also, as time-domain BIOs for the wave equation are written as convolutional operators and their Laplace domain counterparts are BIOs for the modified Helmholtz equation, we will be interested in a method that takes advantage of this relation. CQ lets us approximate convolutions only considering information in the Laplace domain. Moreover, high-order time domain solutions can be achieved by Runge-Kutta discretizations.

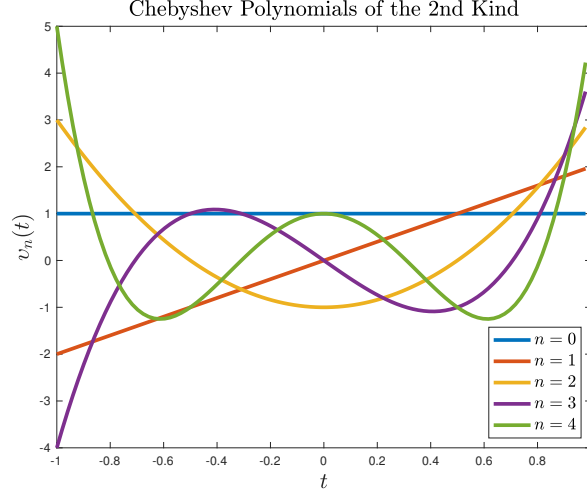


Figure 2: Chebyshev polynomials of the second kind, degrees $n = 0, \dots, 4$.

4.1 Discretization by spectral elements

Following [25, 26], we consider spectral elements to discretize the spatial densities in the MTF for two dimensional problems. We assume that for each interface $\Gamma_{j\ell}$ there exists a C^1 -parametrization $h_{j\ell}$ that maps the nominal segment $\hat{\Gamma} := [-1, 1]$ onto $\Gamma_{j\ell}$. We achieve a non-conforming Petrov-Galerkin discretization of problem (23) by using second kind Chebyshev polynomials of degree $n \in \mathbb{N}_0$:

$$v_n(t) := \frac{\sin(n+1)\theta}{\sin\theta}, \quad t = \cos\theta, \quad \theta \in [0, \pi], \quad (32)$$

as trial functions and weighted second kind Chebyshev polynomials as test functions (see Table 1 for definition). On each interface we use a trial space for both $H^{1/2}(\Gamma_{j\ell})$ and $H^{-1/2}(\Gamma_{j\ell})$ spanned by $\{v_0, \dots, v_n\}$ scaled by the inverse of the Jacobian of the corresponding interface. Their density in the product spaces $\mathbf{V}_{pw,\ell}$ and $\tilde{\mathbf{V}}_\ell$ was established in [25, Propositions 1-2].

We recall the orthogonality property:

$$\int_{-1}^1 v_m(t)v_n(t)\sqrt{1-t^2}dt = \begin{cases} 0 & n \neq m, \\ \pi/2 & n = m, \end{cases} \quad (33)$$

which jointly with related Fourier-Chebyshev expansions [38, Chapter 3] lead to faster matrix entries computations by means of the FFT. Trial and test functions are defined over a whole boundary $\partial\Omega_\ell$ as $\boldsymbol{\xi}_{(n_1, n_2)}^\ell := \sum_{j \in \Upsilon_\ell} \boldsymbol{\xi}_{(n_1, n_2)}^{j\ell} 1_{\Gamma_{j\ell}}$ where $1_{\Gamma_{j\ell}}$ is a characteristic function over the interface $\Gamma_{j\ell}$ and

$$\boldsymbol{\xi}_{(n_1, n_2)}^{j\ell} := \frac{1}{|h'_{j\ell}|} \hat{\boldsymbol{\xi}}_{(n_1, n_2)} \circ h_{j\ell}^{-1}, \quad \hat{\boldsymbol{\xi}}_{(n_1, n_2)}(t) := (v_{n_1}(t), v_{n_2}(t)), \quad t \in \hat{\Gamma}. \quad (34)$$

Similarly, test functions are defined as $\boldsymbol{\chi}_{(n_1, n_2)}^\ell := \sum_{j \in \Upsilon_\ell} \boldsymbol{\chi}_{(n_1, n_2)}^{j\ell} 1_{\Gamma_{j\ell}}$ with

$$\boldsymbol{\chi}_{(n_1, n_2)}^{j\ell} := \frac{1}{|h'_{j\ell}|} \hat{\boldsymbol{\chi}}_{(n_1, n_2)} \circ h_{j\ell}^{-1}, \quad \hat{\boldsymbol{\chi}}_{(n_1, n_2)}(t) := (v_{n_1}(t)\sqrt{1-t^2}, v_{n_2}(t)\sqrt{1-t^2}), \quad t \in \hat{\Gamma}. \quad (35)$$

Trial functions		Test functions	
$H^{\frac{1}{2}}(\widehat{\Gamma})$	$v_n(t)$	$\widetilde{H}^{-\frac{1}{2}}(\widehat{\Gamma})$	$v_n(t)\sqrt{1-t^2}$
$H^{-\frac{1}{2}}(\widehat{\Gamma})$	$v_n(t)$	$\widetilde{H}^{\frac{1}{2}}(\widehat{\Gamma})$	$v_n(t)\sqrt{1-t^2}$

Table 1: Functions used for the spectral elements discretization over $\widehat{\Gamma} = [-1, 1]$.

Letting $\mathbf{X}_L^\ell := \text{span} \left\{ \boldsymbol{\xi}_{(n_1, n_2)}^\ell \right\}_{n_1, n_2=0}^L \subseteq \mathbf{V}_{pw, \ell}$ and $\mathbf{Y}_L^\ell := \text{span} \left\{ \boldsymbol{\chi}_{(n_1, n_2)}^\ell \right\}_{n_1, n_2=0}^L \subseteq \widetilde{\mathbf{V}}_\ell$ for $L \in \mathbb{N}$. Moreover, let

$$\mathbb{X}_{M,L} := \mathbf{X}_L^0 \times \dots \times \mathbf{X}_L^M, \quad \mathbb{Y}_{M,L} := \mathbf{Y}_L^0 \times \dots \times \mathbf{Y}_L^M.$$

We can now define the discrete version of Problem 2.3:

Problem 4.1 (Spectral non-conforming Petrov-Galerkin MTF). *We seek $\boldsymbol{\Lambda}_L \in \mathbb{X}_{M,L}$ such that the variational form:*

$$(\mathbf{F}(s)\boldsymbol{\Lambda}_L, \boldsymbol{\Phi}_L)_\times = (\mathbf{G}, \boldsymbol{\Phi}_L)_\times, \quad \text{for all } \boldsymbol{\Phi}_L \in \mathbb{Y}_{M,L}, \quad (36)$$

is satisfied for $\mathbf{G} = (G_0, G_1, \dots, G_M) \in \mathbb{V}_{pw, M}$.

Existence and uniqueness of solutions for Problem 4.1 depends on the existence of an inf-sup condition. This result remains elusive by now, but various numerical experiments show the good behaviour of the proposed discretization scheme [25, 26].

Remark 4.2. *Notice that the discrete problem consists in finding a solution in the space $\mathbb{V}_{pw, M}$ instead of \mathbb{V}_M , which was the case for Problem 2.3. Existence and uniqueness for the continuous problem remains valid in $\mathbb{V}_{pw, M}$, as mentioned in [25, Theorem 1], due to the equivalence of the duality product between \mathbb{V}_M and $\mathbb{V}_{pw, M}$ when test functions are elements of $\widetilde{\mathbb{V}}_M$.*

4.2 Computation of BIOs

We now show the explicit integrals computed for each of the BIOs involved in the construction of the Calderón operator, as it was done in [25]. Integrals over $\widehat{\Gamma} \times \widehat{\Gamma}$ are numerically approximated in the following two-step scheme:

- (a) Computation of Chebyshev coefficients for the kernel in the inner integral.
- (b) Gauss-Legendre quadrature rule for the outer integral.

For implementation purposes, we briefly explain the algorithm. Let $K(t, \tau) : \widehat{\Gamma} \times \widehat{\Gamma} \rightarrow \mathbb{C}$ denote any of the BIO kernels. For each subdomain Ω_ℓ and for a pair of interfaces $\Gamma_{j\ell}$ and $\Gamma_{k\ell}$, we proceed as follows:

- i. Set the number of Gauss-Legendre quadrature points $\{t_j\}_{j=1}^{N_g}$ and Chebyshev points $\{\tau_l\}_{l=1}^{N_c}$.
- ii. Kernels $K(t, \tau)$ are evaluated at each of these points and their values are stored. For $j = k$ the kernel is regularized with the Laplace kernel to extract the singularity (see Remark 4.3).

iii. By means of the FFT over a periodization of the array $\{K(t_j, \tau_l)\}_{l=1}^{N_c}$, one computes approximations of the Chebyshev coefficients $f_n(t_j)$, $n = 1, \dots, N_c$ associated to the kernel

$$K(t_j, \tau) \approx \sum_{n=0}^{N_c} f_n(t_j) v_n(\tau)$$

for every Gauss-Legendre quadrature point t_j , $j = 1, \dots, N_g$.

iv. The outer integral is computed via a Gauss-Legendre quadrature rule.

4.2.1 Weakly Singular BIO

For the weakly singular operator $V_\ell(s)$, $s \in \mathbb{C}_+$ defined on the boundary $\partial\Omega_\ell$ we need to compute integrals of the form:

$$\int_{\hat{\Gamma}} \int_{\hat{\Gamma}} G_\ell(\|h_{\ell j}(\tau) - h_{\ell k}(t)\|; s) v_l(t) v_m(\tau) \sqrt{1 - \tau^2} d\tau dt. \quad (37)$$

For $t \neq \tau$ we have the approximation:

$$G_\ell(\|h_{\ell j}(\tau) - h_{\ell k}(t)\|; s) \approx \sum_{n=0}^N f_n(t) v_n(\tau) \quad (38)$$

and by the orthogonality property (33) we obtain

$$\int_{\hat{\Gamma}} \int_{\hat{\Gamma}} G_\ell(\|h_{\ell j}(\tau) - h_{\ell k}(t)\|; s) v_l(t) v_m(\tau) \sqrt{1 - \tau^2} d\tau dt \approx \frac{\pi}{2} \int_{-1}^1 f_l(t) v_l(t) dt \quad (39)$$

which is then approximated by a Gauss-Legendre quadrature rule.

4.2.2 Double Layer BIOs

For the double layer BIO $K_\ell(s)$ and adjoint BIO $K'_\ell(s)$ defined on the boundary $\partial\Omega_\ell$ the procedure follows the same way as Section 4.2.1. The only difference is that the Chebyshev coefficients have to be computed on a different kernel.

4.2.3 Hypersingular BIO

For the hypersingular operator $W_\ell(s)$ defined on the boundary $\partial\Omega_\ell$ we employ the following expression from [37, Lemma 6.13, Theorem 6.15]. Let Γ be an open part of $\partial\Omega_\ell$ and f and g continuously differentiable on Γ . Then

$$\begin{aligned} \langle W_\ell(s) f, g \rangle_\Gamma &= \langle V_\ell(s) \operatorname{curl} f, \operatorname{curl} g \rangle_\Gamma + \left(\frac{s}{c_\ell} \right)^2 \langle V_\ell(\mathbf{n}_\mathbf{x}^\ell \cdot \mathbf{n}_\mathbf{y}^\ell f), g \rangle_\Gamma \\ &\quad - f(\mathbf{x}) \int_\Gamma G_\ell(\|\mathbf{x} - \mathbf{y}\|; s) \operatorname{curl} g(\mathbf{y}) d\Gamma_\mathbf{y} \Big|_{\mathbf{x} \in \partial\Gamma} \end{aligned} \quad (40)$$

The first and second terms are computed based on the weakly singular BIO and derivatives of Chebyshev polynomials. The third term involves computing Chebyshev coefficients and no quadrature rule is required.

Remark 4.3. Regularization of the kernel is done for the case $\Gamma_{j\ell} = \Gamma_{k\ell}$ by using the Laplace kernel

$$G(\mathbf{x}, \mathbf{y}) := \frac{1}{2\pi} \log |\mathbf{x} - \mathbf{y}|, \quad \mathbf{x} \neq \mathbf{y}.$$

A known expansion of this kernel based on Chebyshev polynomials of the first kind T_n simplifies our computations:

$$\frac{1}{2\pi} \log(|t - \tau|) = \frac{1}{2\pi} \log 2 + \sum_{n=1}^{\infty} \frac{1}{n\pi} T_n(t) T_n(\tau), \quad \tau \neq t \in \widehat{\Gamma}.$$

Two integrals have to be computed: one with the regularized kernel $G_\ell(\mathbf{x}, \mathbf{y}; s) - G(\mathbf{x}, \mathbf{y})$ and one with the Laplace kernel computed precisely.

5 Convolution Quadrature

Multistep-based and multistage CQ were introduced by Lubich in [29, 30] and in [31], respectively. Both methods will be explained along with their assumptions and limitations, following the presentation given in [19].

Consider two functions $f : [0, \infty) \rightarrow \mathcal{X}$ and $g : [0, \infty) \rightarrow \mathcal{Y}$ where \mathcal{X} and \mathcal{Y} are normed spaces. We also assume that $F(s) := (\mathcal{L}f)(s)$ is known. We are interested in computing their convolution, which corresponds to

$$h(t) := \int_0^t f(\tau) g(t - \tau) d\tau = \frac{1}{2\pi i} \int_{\sigma - i\infty}^{\sigma + i\infty} F(s) \left(\int_0^t e^{s\tau} g(t - \tau) d\tau \right) ds. \quad (41)$$

The inner integral in the right-hand side corresponds to the exact solution of an ODE

$$\dot{y}(t) = sy(t) + g(t) \quad t \in \mathbb{R}_+, \quad y(0) = 0, \quad (42)$$

which can be solved by means of a multistep or a multistage linear method.

5.1 Multistep Convolution Quadrature

A multistep method [40, Ch. III.2] for solving equation (42) is defined by parameters α_ℓ, β_ℓ , $\ell = 0, \dots, m$ and a timestep $\Delta t > 0$ with discrete times $t_n = n\Delta t$ such that the new unknown corresponds to $y_n \approx y(t_n)$, $n = 0, 1, \dots$ in

$$\sum_{\ell=0}^m \alpha_\ell y_{n+\ell-m} = \Delta t \sum_{\ell=0}^m \beta_\ell (s y_{n+\ell-m} + g_{n+\ell-m}), \quad n = 0, 1, \dots \quad (43)$$

The Z -transform applied on the previous expression leads to a new equation in the Z -domain:

$$Y(\zeta) := \sum_{n=0}^{\infty} y_n \zeta^n = \frac{1}{\frac{1}{\Delta t} \delta(\zeta) - s} G(\zeta), \quad (44)$$

where $\delta(\zeta) = \frac{\sum_{\ell=0}^m \alpha_{m-\ell} \zeta^\ell}{\sum_{\ell=0}^m \beta_{m-\ell} \zeta^\ell}$ and $G(\zeta) = \sum_{n=0}^{\infty} g_n \zeta^n$. Using an A-stable method will ensure that the rational polynomial δ satisfies $\delta(\zeta) \in \mathbb{C}_+$ for $|\zeta| < 1$. [29, Section 1, p.131]. Inserting the solution (44) into (41) for discrete times $t_n = n\Delta t$, $n = 0, 1, \dots$, and denoting this approximation $\tilde{h}(t)$, we obtain

$$\tilde{h}(t_n) = \frac{1}{2\pi i} \int_{\mathcal{C}} \frac{1}{\zeta^{n+1}} F\left(\frac{\delta(\zeta)}{\Delta t}\right) G(\zeta) d\zeta, \quad (45)$$

which is well defined considering the analyticity of F, G and δ . The contour \mathcal{C} must belong to the analyticity region of the transfer function $F\left(\frac{\delta(\zeta)}{\Delta t}\right) G(\zeta)$ and wind around 0 once [29]. The right-hand side in (45) can be computed by noticing that

$$F\left(\frac{\delta(\zeta)}{\Delta t}\right) = \sum_{n=0}^{\infty} \omega_n^F(\Delta t) \zeta^n, \quad G(\zeta) = \sum_{n=0}^{\infty} g_n \zeta^n, \quad F\left(\frac{\delta(\zeta)}{\Delta t}\right) G(\zeta) = \sum_{n=0}^{\infty} \sum_{m=0}^n \omega_m^F(\Delta t) g_{n-m} \zeta^m \quad (46)$$

concluding that

$$\tilde{h}(t_n) = \sum_{m=0}^n \omega_m^F(\Delta t) g_{n-m}, \quad (47)$$

where the so-called CQ weights $\omega_n^F(\Delta t), n = 0, 1, \dots$, can be computed by applying the inverse Z-transform. For implementation purposes, a good choice for the contour of integration \mathcal{C} is a circle of radius $\lambda < 1$, explicitly $\lambda = \varepsilon^{\frac{1}{2N}}$ [7], where ε is the machine number. This allows the stable use of FFT to compute the integral by means of a trapezoidal rule. Following [19, Sections 3.2-3.3], the final expression is

$$\frac{1}{2\pi i} \int_{\mathcal{C}} \frac{1}{\zeta^{n+1}} F\left(\frac{\delta(\zeta)}{\Delta t}\right) G(\zeta) d\zeta \approx \lambda^{-n} \left(\frac{1}{N+1} \sum_{\ell=0}^N \hat{F}_{\ell} \left(\sum_{m=0}^N \lambda^m g_m \zeta_{N+1}^{-m\ell} \right) \zeta_{N+1}^{\ell n} \right), \quad (48)$$

where $\hat{F}_{\ell} = F\left(\frac{\delta(\lambda \zeta_{N+1}^{-\ell})}{\Delta t}\right)$, $\zeta_{N+1} = e^{\frac{2\pi i}{N+1}}$ and $N \in \mathbb{N}$ is the number of quadrature points in the trapezoidal rule. The order of convergence of this method is that of the multistep method chosen. Due to Dahlquist's barrier theorem [39], A-stable multistep methods are limited to order less than or equal to two, which is the main disadvantage of multistep based CQ.

5.2 Multistage Convolution Quadrature

There are A-stable implicit multistage methods of arbitrary order [4]. This is the main motivation for considering them for solving (42) instead of multistep methods. Letting $A \in \mathbb{R}^{m \times m}$, $\mathbf{b}, \mathbf{d} \in \mathbb{R}^m$ be the Butcher tableau for a given m -stage Runge-Kutta method [39, Chapter 4], and defining $y_{nj} \approx y(t_n + d_j \Delta t)$, the problem consists in looking for a vector-valued function $\mathbf{y}_n := (y_{n1}, \dots, y_{nm}) = (y(t_n + d_1 \Delta t), \dots, y(t_n + d_m \Delta t)) = y(t_n + \mathbf{d} \Delta t)$, $n = 0, \dots, N$ of stage solutions such that

$$\begin{aligned} \mathbf{y}_n &= \mathbf{y}_n \mathbf{1} + \Delta t A (\mathbf{y}_n + g(t_n + \mathbf{d} \Delta t)), \\ \mathbf{y}_{n+1} &= \mathbf{y}_n + \Delta t \mathbf{b} \cdot (\mathbf{y}_n + g(t_n + \mathbf{d} \Delta t)). \end{aligned} \quad (49)$$

Letting $\mathbf{Y}(\zeta) = \sum_{n=0}^{\infty} \mathbf{y}_n \zeta^n$, $\mathbf{G}(\zeta) = \sum_{n=0}^{\infty} g(t_n + \mathbf{d} \Delta t) \zeta^n$ and $\delta^{\text{RK}}(\zeta) := \left(\mathbf{1} \mathbf{b}^T \frac{\zeta}{1-\zeta} + A \right)^{-1}$, following a similar procedure as the multistep case [4] it is possible to obtain

$$\mathbf{Y}(\zeta) = \left(\frac{\delta^{\text{RK}}(\zeta)}{\Delta t} - sI \right)^{-1} \mathbf{G}(\zeta). \quad (50)$$

Recalling that

$$\mathbf{H}(\zeta) = F\left(\frac{\delta^{\text{RK}}(\zeta)}{\Delta t}\right) \mathbf{G}(\zeta) \quad (51)$$

implies that

$$\mathbf{h}_n = h(t_n + \mathbf{d}\Delta t) = \Delta t \sum_{k=0}^n W_{n-k} g(t_k + \mathbf{d}\Delta t), \quad (52)$$

wherein $F\left(\frac{\delta^{\text{RK}}(\zeta)}{\Delta t}\right) = \Delta t \sum_{n=0}^{\infty} W_n \zeta^n$, $\mathbf{G}(\zeta) = \sum_{n=0}^{\infty} g(t_n + \mathbf{d}\Delta t) \zeta^n$ and $W_n \in \mathbb{R}^{m \times m}$ the matricial convolution weights. If we consider stiffly accurate Runge-Kutta methods –for example RadauIIA or LobattoIIIC classes [31]– we have the relation $h_{nm} = h_{n+1}$. The procedure to obtain the convolution at each discrete time follows the same idea for the approximation (48).

In [4, Theorem 3.2], one finds an error estimate

$$|\tilde{h}(t_n) - h(t_n)| = \mathcal{O}\left(\Delta t^{\min(p, q+1-\mu_2)}\right),$$

where p and q are the classical and stage order of convergence of the Runge-Kutta method and $\mu_2 \in \mathbb{R}$ is a constant related to the transfer function $F(s)$ (see [4, Assumption 2.1 and Lemma 2.2]).

5.3 Convolutional Equations

We have shown how to compute convolutions with CQ, but we are interested in solving equations where the unknown is one of the terms involved in the convolution. As explained in Sections 5.1 and 5.2, convolutions can be computed as (47) or (51), depending if a multistep or multistage method is used. From now on, we follow the notation of multistep methods for the sake of simplicity, but exactly the same procedure works for multistage ones.

Problem 5.1 (CQ-MTF). *Let $N \in \mathbb{N}$, $\Delta t = T/N > 0$ be the timestep chosen for a CQ scheme, $T > 0$ the final time of computation and $t_m = m\Delta t$ discrete times for $m = 0, \dots, N$. Let $\delta(\zeta)$ be given by the choice of a multistep or multistage A-stable method. We look for solutions $\lambda_m \in \mathbb{V}_{pw, M}$ at each t_m , $m = 0, \dots, N$, such that*

$$\left(\sum_{m=0}^n \omega_m^F(\Delta t) \lambda_{n-m}, \Phi \right)_{\times} = (\mathbf{g}(t_n), \Phi)_{\times}, \quad \text{for all } \Phi \in \tilde{\mathbb{V}}_M, \quad (53)$$

where $\omega_m^F(\Delta t)$ are the CQ weights coming from the analytic expansion (46), F is the multiple traces operator defined in Problem 2.3 and $\mathbf{g}(t)$ is the boundary data defined in Problem 3.2.

As Problem 5.1 corresponds to a triangular Toeplitz system, existence and uniqueness of solutions depend on the solvability of the diagonal terms

$$(\omega_0^F(\Delta t) \lambda, \varphi)_{\times} = (\Xi, \Phi)_{\times}, \quad \text{for all } \Phi \in \tilde{\mathbb{V}}_M, \quad (54)$$

for a given $\Xi \in \mathbb{V}_{pw, M}$. The convolution weights satisfy [19]

$$\omega_n^F(\Delta t) = \frac{1}{n!} \frac{d^n}{d\zeta^n} \left(F\left(\frac{\delta(\zeta)}{\Delta t}\right) \right) \Big|_{\zeta=0}, \quad n = 0, \dots, N,$$

and so $\omega_0^F(\Delta t) = F\left(\frac{\delta(0)}{\Delta t}\right)$, for which we have existence and uniqueness of solutions for (54) since $\delta(0) \in \mathbb{C}_+$.

Theorem 5.2. *There exists a unique solution $\{\boldsymbol{\lambda}_n\}_{n=0}^N \in [\mathbb{V}_{pw,M}]^{N+1}$ for Problem 5.1.*

Proof. Problem 5.1 can be written as a Toeplitz system:

$$\begin{pmatrix} (\omega_0^F(\Delta t)\boldsymbol{\lambda}_0, \boldsymbol{\varphi})_{\times} & \dots & 0 & = & (\mathbf{g}(t_0), \boldsymbol{\varphi})_{\times}, \\ \vdots & \ddots & \vdots & & \vdots \\ (\omega_N^F(\Delta t)\boldsymbol{\lambda}_0, \boldsymbol{\varphi})_{\times} & + \dots + & (\omega_0^F(\Delta t)\boldsymbol{\lambda}_N, \boldsymbol{\varphi})_{\times} & = & (\mathbf{g}(t_N), \boldsymbol{\varphi})_{\times}, \end{pmatrix}$$

for all $\boldsymbol{\varphi} \in \widetilde{\mathbb{V}}_M$. As (54) has a unique solution in $\mathbb{V}_{pw,M}$ for every right-hand side $\boldsymbol{\Xi} \in \mathbb{V}_{pw,M}$, each one of the previous equations is uniquely solvable by $\boldsymbol{\lambda}_n$, $n = 0, \dots, N$, by Theorem 2.6. \square

Finally, the fully discrete problem reads as follows:

Problem 5.3 (Fully Discrete CQ-Spectral Galerkin MTF). *Let $N \in \mathbb{N}$, $\Delta t = T/N > 0$ be the timestep chosen for a CQ scheme, $T > 0$ the final time of computation and $t_0 = 0, t_1 = \Delta t, \dots, t_m = m\Delta t, \dots, t_N = T$ discrete times. Let $\delta(\zeta)$ be given by the choice of a multistep or multistage A-stable method. We look for solutions $\boldsymbol{\lambda}_m \in \mathbb{X}_{M,L}$ at each discrete time t_m , $m = 0, \dots, N$, such that*

$$\left(\sum_{m=0}^n \omega_m^F(\Delta t)\boldsymbol{\lambda}_{n-m}, \boldsymbol{\varphi} \right)_{\times} = (\mathbf{g}(t_n), \boldsymbol{\varphi})_{\times}, \quad \text{for all } \boldsymbol{\varphi} \in \mathbb{Y}_{M,L}, \quad (55)$$

where $\omega_m^F(\Delta t)$, $m = 0, \dots, N$ are the CQ weights coming from the analytic expansion (46), \mathbf{F} is the multiple traces operator defined in Problem 2.3 and $\mathbf{g}(t)$ is the boundary data defined in Problem 3.2.

Well-posedness of Problem 5.3 follows closely the arguments used for the proof of Theorem 5.2.

6 Numerical Experiments

We present several numerical experiments to validate our method for different scenarios. All computations were performed on MATLAB 2018a, 64bit, running on a GNU/Linux desktop machine with a 3.80 GHz CPU and 32GB RAM.¹ We measure different error norms to verify that our implementation is correct and reveal its performance. We use equivalent norms for the spaces $H^{\pm\frac{1}{2}}(\Gamma)$ based on the single layer operator and its inverse, for a wavenumber $k = 10i$ ($s = 10$ for modified Helmholtz equation).

For each numerical example, we compute relative trace errors over each interface for a density $\varphi \in H^s(\Gamma_\ell)$ compared to a reference density $\varphi^{\text{ref}} \in H^s(\Gamma_\ell)$, with $s \in \{-\frac{1}{2}, \frac{1}{2}\}$. We express it as follows

$$\text{TraceError}(\Gamma_\ell) := \frac{\left(\sum_{n=0}^N \|\varphi_n^{\text{ref}} - \varphi_n\|_{H^s(\Gamma_\ell)}^2 \right)^{\frac{1}{2}}}{\left(\sum_{n=0}^N \|\varphi_n^{\text{ref}}\|_{H^s(\Gamma_\ell)}^2 \right)^{\frac{1}{2}}}, \quad \ell = 0, 1, \dots, M. \quad (56)$$

We also compute field errors over sample points X in each domain Ω_ℓ by using the representation formula (11), compared to a reference field u^{ref}

¹The code is available in <http://www.github.com/ijlabarca/cqmtf>.

Method	Stages	Stage order (q)	Classical order (p)
Radau IIA	s	s	$2s - 1$
Lobatto IIIC	s	$s - 1$	$2s - 2$

Table 2: Properties of Runge-Kutta methods used for CQ[39, Chapter 7].

$$\text{ErrorU}(\Omega_\ell) := \frac{\left(\sum_{n=0}^N \sum_{\mathbf{x} \in X} |u_n^{\text{ref}}(\mathbf{x}) - u_n(\mathbf{x})|^2 \right)^{\frac{1}{2}}}{\left(\sum_{n=0}^N \sum_{\mathbf{x} \in X} |u_n^{\text{ref}}(\mathbf{x})|^2 \right)^{\frac{1}{2}}}, \quad X \subset \Omega_\ell. \quad (57)$$

CQ is implemented using the BDF2 multistep method [39, Chapter 5], completely determined by the polynomial

$$\gamma(\zeta) = \frac{3}{2} - 2\zeta + \frac{1}{2}\zeta^2, \quad (58)$$

and multistage methods (Runge-Kutta CQ) corresponding to the two-stage RadauIIa quadrature [39, Chapter 7], whose Butcher's tableau is defined by

$$A := \begin{pmatrix} 5/12 & -1/12 \\ 3/4 & 1/4 \end{pmatrix}, \quad \mathbf{b} := \begin{pmatrix} 3/4 \\ 1/4 \end{pmatrix} \quad \text{and} \quad \mathbf{d} := \begin{pmatrix} 1/3 \\ 1 \end{pmatrix}, \quad (59)$$

and the three-stage LobattoIIIC quadrature [39, Chapter 7], whose Butcher's tableau is defined by

$$A := \begin{pmatrix} 1/6 & -1/3 & 1/6 \\ 1/6 & 5/12 & -1/12 \\ 1/6 & 2/3 & 1/6 \end{pmatrix}, \quad \mathbf{b} := \begin{pmatrix} 1/6 \\ 2/3 \\ 1/6 \end{pmatrix} \quad \text{and} \quad \mathbf{d} := \begin{pmatrix} 0 \\ 1/2 \\ 1 \end{pmatrix}. \quad (60)$$

Properties of the Radau IIA and Lobatto IIIC methods are summarized in Table 2. It is important to notice the differences among these as they play an important role in the expected order of convergence in the numerical scheme. The best result that one can expect is the classical order of convergence p , which is 2.0 for the BDF2 method and depends on the number of stages for Runge-Kutta methods. Order reduction phenomena are also common and has been observed for other wave propagation problems and CQ applications [4, 6, 35]. In general, this depends on the stage order q , which in our case is the same for RadauIIA and LobattoIIIC. Recall that we do not provide numerical estimates and regularity results for the solutions of wave propagation problems over composite materials. Thus, we cannot claim more precise bounds other than these lower and upper ones for error convergence in time domain.

6.1 Spectral discretization with Chebyshev polynomials

First, we show convergence results for the non-conforming spectral discretization presented in Section 4.1. Although we are using a spectral non-conforming discretization with Chebyshev polynomials, convergence rates are not expected to be exponential. This is related to the regularity of solutions of Helmholtz transmission problems in non-smooth domains [18]. Our aim is to show that we still obtain high-order convergence rates with accurate solutions using only a relatively small number of degrees of freedom. This will be useful to set an appropriate number of Chebyshev polynomials in the next sections.

Table 3: Parameters used for Example in Section 6.1. Convergence results are shown in Figure 4.

	s_0	s_1	s_2	U^{inc}	\mathbf{d}
Example A (blue)	$-i$	$-2i$	$-4i$	$\exp(-s_0 \mathbf{x} \cdot \mathbf{d})$	$(0, -1)$
Example B (green)	$1 - i$	$2 - 2i$	$4 - 4i$	$\exp(-s_0 \mathbf{x} \cdot \mathbf{d})$	$(0, -1)$
Example C (brown)	$1 - i$	$10 - 10i$	$20 - 20i$	$\exp(-s_0 \mathbf{x} \cdot \mathbf{d})$	$(0, -1)$
Example D (purple)	$1 - i$	$10 - 10i$	$100 - 100i$	$\exp(-s_0 \mathbf{x} \cdot \mathbf{d})$	$(0, -1)$

c_0	c_1	ω	T	t_{lag}	\mathbf{d}	N_{cheb}
1	0.5	1	5	0.5	$(1, 0)$	40

Table 4: Parameters used for Example in Section 6.2.

We solve Problem 2.3 for a domain given by the circle with radius $r = 0.5$ with two subdomains (see Figure 3a). The volume problem to be solved by the multiple traces formulation in these examples corresponds to

$$\begin{cases} -\Delta U + s_\ell^2 U = 0 & \text{in } \Omega_\ell, \ell = 0, 1, 2, \\ \llbracket \gamma U \rrbracket_{0\ell} = -\gamma U^{\text{inc}}|_{\Gamma_{0\ell}}, & \ell = 1, 2, \\ \llbracket \gamma U \rrbracket_{12} = 0, \\ \llbracket \gamma U \rrbracket_{21} = 0, \end{cases} \quad (61)$$

Parameters employed are shown in Table 3 with error convergence results measured with respect to a highly resolved solution displayed in Figure 4 considering traces and resulting volume fields. Different values of s are used in order to observe errors for different problems. As expected, solutions start by having a spectrally accurate behaviour but they eventually reach a polynomial convergence rate due to the non-smoothness of the domains. Small errors are obtained with few polynomials, which is good in terms of BDF2 and two-stage RadauIIA CQ methods that will be used in the next sections. For LobattoIIIc a higher number of polynomials is required due to its high order convergence in time, so for the next examples in the time-domain we fix the number of polynomials to prevent having errors due to the frequency domain solver. Error estimates for the solution obtained for modified Helmholtz equations could be useful in the future to develop adaptivity in terms of number of Chebyshev polynomials. This remains open for real wavenumbers [25] and for complex wavenumbers.

6.2 Manufactured time-domain solutions with no triple points

We now analyze our time-domain CQ-MTF by considering the case of a single domain, i.e. no triple points. The domain Ω consists of a circle of radius $r = 0.5$. We construct transmission conditions such that the exterior solution is zero and the interior solution corresponds to

$$u_1(\mathbf{x}, t) := f(c_1 t - t_{\text{lag}} - \mathbf{x} \cdot \mathbf{d}), \quad f(t) := \sin(\omega t) \eta(t, 0.2, 2), \quad \ell = 1, 2, \quad (62)$$

where the parameters used are shown in Table 4 and η is a smooth version of the Heaviside function defined by

$$\eta(t, t_0, t_1) := \begin{cases} 0 & 0 \leq t < t_0, \\ 1 - \exp\left(\frac{2e^{-1/\tau}}{\tau - 1}\right), \quad \tau = \frac{t - t_0}{t_1 - t_0}, & t_0 < t < t_1, \\ 1 & t > t_1. \end{cases} \quad (63)$$

Convergence results for BDF2 and Runge-Kutta CQ methods are shown in Figure 6. Classical order of convergence is restricted to the exterior domain whereas for interior ones, CQ methods suffer from reduced convergence rates. We observe that the three implemented methods share the same convergence rates for Neumann traces. This is explained by the regularity of the solutions, as normally the methods would portray different orders.

6.3 Manufactured time-domain solutions with artificial subdomains

We now validate the use of CQ-MTF by considering the case of artificial subdomains. The domain Ω consists in a circle of radius $r = 0.5$ separated into two subdomains Ω_1 and Ω_2 –left and right semicircles, respectively in Figure 3a. We use the same manufactured solutions from Section 6.2. As the physical parameters of both subdomains are identical, the only difference from the case in Section 6.2 is the presence of an artificial triple point.

As before, error convergence results for BDF2 and Runge-Kutta-based CQ (RadauIIa and LobattoIIIc) are shown in Figure 6. Only small differences can be pointed out with respect to the results of Section 6.2, in particular with the convergence of Neumann traces, which seems to improve for RadauIIa. However, these results are not enough to state that increasing the number of subdomains artificially impacts the convergence of the method.

6.4 Incident plane wave over a circle with two subdomains

We now consider as incident field a plane wave coming from Ω_0 , defined by

$$u^{\text{inc}}(\mathbf{x}, t) = f(c_0(t - t_{\text{lag}}) - \mathbf{x} \cdot \mathbf{d}), \quad f(t) = \sin(\omega t)\eta(t, 0.2, 2). \quad (64)$$

The domain is a circle of radius $r = 0.5$ divided into two subdomains from Figure 3a. The parameters used are shown in Table 6.

Error convergence results with respect to a highly resolved solution for each subdomain are shown in Figure 7. We observe that the second order convergence for the BDF2 method is not achieved until a high number of timesteps is reached due to the highly oscillatory incident field. Runge-Kutta methods show the expected order of convergence for the Dirichlet trace and for the scattered field, having even better results for the case of RadauIIa. Neumann traces present a slower convergence, as it was the case for previous examples. This behaviour is related to the stage order of convergence in Runge-Kutta methods, which is the same for two-stages RadauIIa and three-stages LobattoIIIc ($q = 2$). Some snapshots of the solution are shown in Figure 8.

6.5 Incident plane wave over a Square with four subdomains

The incident field is the same plane wave from (64) coming from Ω_0 . Parameters used are $t_{\text{lag}} = 0.5$, $\mathbf{d} = (\sqrt{0.5}, -\sqrt{0.5})$ and $\omega = 8$. The domain is a square with side length $a = 1$ divided into four subdomains (see Figure 3b). Wavespeeds on each subdomain are $c_0 = 1, c_1 = 0.5, c_2 = 0.25, c_3 = 0.5, c_4 = 0.25$.

Convergence results for each interface are shown in Figure 9. We observe a similar behaviour to the previous example, with slow convergence for the BDF2 method. Snapshots of the volume solution are displayed in Figure 10.

c_0	c_1	c_2	ω	T	t_{lag}	\mathbf{d}	N_{cheb}
1	0.5	0.5	1	5	0.5	(1, 0)	40

Table 5: Parameters used for Example in Section 6.3.

Table 6: Parameters used for Example in Section 6.4.

c_0	c_1	c_2	ω	T	t_{lag}	\mathbf{d}	N_{cheb}
1	0.5	0.25	8	10	0.5	$(\sqrt{0.5}, -\sqrt{0.5})$	80

Table 7: Parameters used for Example in Section 6.5.

c_0	c_1	c_2	c_3	c_4	ω	T	t_{lag}	\mathbf{d}	N_{cheb}
1	0.5	0.25	0.5	0.25	8	10	0.5	$(\sqrt{0.5}, -\sqrt{0.5})$	20

6.6 Incident plane wave over kite with two subdomains

The incident field is the same plane wave from (64) coming from Ω_0 . The domain is a kite parametrized by

$$\begin{pmatrix} x(t) \\ y(t) \end{pmatrix} = \begin{pmatrix} \cos(t) + 0.65 \cos(2t) \\ \sin(t) \end{pmatrix}, \quad t \in [0, 2\pi] \quad (65)$$

divided into two subdomains Ω_1 and Ω_2 (corresponding to upper and lower halves) with symmetry over the x -axis. Parameters used are shown in Table 8. Convergence results for each interface are shown in Figure 11. Snapshots of the volume solution are displayed in Figure 12.

7 Concluding remarks

We solve acoustic wave transmission problems over composite scatterers by means of CQ method and the local MTF. We showed that Runge-Kutta CQ constitutes an efficient and accurate method, preferable to multistep methods for their higher order convergence rates. Although reduced order can be expected, this was only reported for convergence of Neumann traces. For every example, convergence of two-stage Radau and three-stage Lobatto coincides for Neumann traces, which can be explained with the fact that both methods have exactly the same stage order $q = 2$.

The use of high-order solvers for frequency domain problems remains mandatory in order to achieve accurate results and take advantage of the capabilities of Runge-Kutta methods. This is achieved in space over open interfaces using Chebyshev polynomials as basis and test functions. These are also suitable functions for the framework of piecewise/broken Sobolev spaces defined over the boundary of each subdomain.

Future work is focused on developing a convergence theory for this formulation. Although very important advances have been made in previous works in [20, 33, 34, 35], the current theoretical framework is well suited only for Galerkin-BEM on standard Sobolev spaces over the boundary of Lipschitz domains, with no clear extension to piecewise or broken spaces considered for trial and test functions in the MTF, or even the Petrov-Galerkin formulation. Numerically, efforts are set towards implementing a three-dimensional version of the presented scheme.

Acknowledgments

This research was funded by FONDECYT Regular 1171491.

Table 8: Parameters used for Example in Section 6.6.

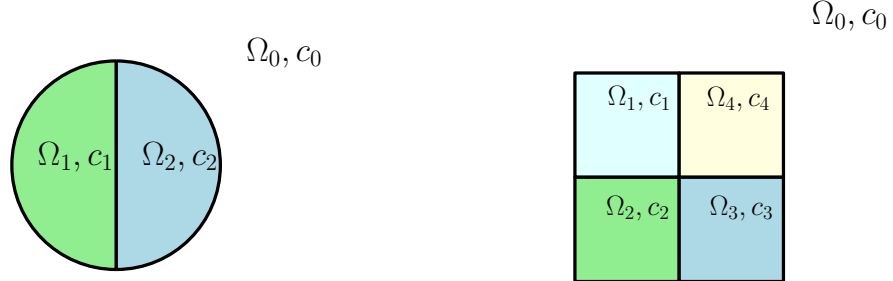
c_0	c_1	c_2	ω	T	t_{lag}	\mathbf{d}	N_{cheb}
1	0.5	0.25	8	10	0.5	(1, 0)	80

References

- [1] A. Aimi, M. Diligenti, C. Guardasoni, I. Mazzieri, and S. Panizzi. An energy approach to space–time Galerkin BEM for wave propagation problems. *International journal for numerical methods in engineering*, 80(9):1196–1240, 2009.
- [2] L. Banjai and M. Kachanovska. Fast Convolution Quadrature for the Wave Equation in three dimensions. *Journal of Computational Physics*, 279:103–126, 2014.
- [3] L. Banjai and C. Lubich. An error analysis of Runge–Kutta Convolution Quadrature. *BIT Numerical Mathematics*, 51(3):483–496, 2011.
- [4] L. Banjai, C. Lubich, and J. M. Melenk. Runge–Kutta Convolution Quadrature for operators arising in Wave propagation. *Numerische Mathematik*, 119(1):1–20, 2011.
- [5] L. Banjai, C. Lubich, and F.-J. Sayas. Stable numerical coupling of exterior and interior problems for the wave equation. *Numerische Mathematik*, 129(4):611–646, 2015.
- [6] L. Banjai, M. Messner, and M. Schanz. Runge–Kutta Convolution Quadrature for the Boundary Element Method. *Computer methods in applied mechanics and engineering*, 245:90–101, 2012.
- [7] L. Banjai and S. Sauter. Rapid Solution of the Wave Equation in Unbounded Domains. *SIAM Journal on Numerical Analysis*, 47(1):227–249, 2008.
- [8] L. Banjai and M. Schanz. Wave propagation problems treated with Convolution Quadrature and BEM. In *Fast Boundary Element Methods in Engineering and Industrial Applications*, pages 145–184. Springer, 2012.
- [9] J.-P. Berenger. A perfectly matched layer for the absorption of electromagnetic waves. *Journal of Computational Physics*, 114(2):185–200, 1994.
- [10] X. Claeys, R. Hiptmair, and C. Jerez-Hanckes. Multitrace Boundary Integral Equations. In *Direct and inverse problems in wave propagation and applications*, volume 14 of *Radon Ser. Comput. Appl. Math.*, pages 51–100. De Gruyter, Berlin, 2013.
- [11] X. Claeys, R. Hiptmair, C. Jerez-Hanckes, and S. Pintarelli. Novel Multi-Trace Boundary Integral Equations for Transmission Boundary Value Problems. In A. S. Fokas and B. Pelleroni, editors, *Unified Transform for Boundary Value Problems: Applications and Advances*, pages 227–258. Philadelphia, SIAM, 2015.
- [12] X. Claeys, R. Hiptmair, and E. Spindler. A second-kind Galerkin Boundary Element method for scattering at composite objects. *BIT Numerical Mathematics*, 55(1):33–57, 2015.
- [13] P. J. Davies. A stability analysis of a time marching scheme for the general surface electric field integral equation. *Applied Numerical Mathematics*, 27(1):33–57, 1998.
- [14] P. J. Davies and D. B. Duncan. Averaging techniques for time-marching schemes for retarded potential integral equations. *Applied Numerical Mathematics*, 23(3):291–310, 1997.

- [15] P. J. Davies and D. B. Duncan. Stability and convergence of collocation schemes for retarded potential integral equations. *SIAM Journal on Numerical Analysis*, 42(3):1167–1188, 2004.
- [16] P. J. Davies, D. B. Duncan, and B. Zubik-Kowal. The stability of numerical approximations of the time domain current induced on thin wire and strip antennas. *Applied numerical mathematics*, 55(1):48–68, 2005.
- [17] S. Eberle, F. Florian, R. Hiptmair, and S. Sauter. A Stable Boundary Integral Formulation of an Acoustic Wave Transmission Problem with Mixed Boundary Conditions. Preprint arXiv:1907.01738 [math.NA], arXiv, 2019. submitted to SIMA.
- [18] P. Grisvard. *Elliptic problems in nonsmooth domains*. SIAM, 2011.
- [19] M. Hassell and F.-J. Sayas. Convolution Quadrature for Wave simulations. In *Numerical simulation in physics and engineering*, pages 71–159. Springer, 2016.
- [20] M. E. Hassell, T. Qiu, T. Sánchez-Vizuet, F.-J. Sayas, et al. A new and improved analysis of the time domain boundary integral operators for the acoustic wave equation. *Journal of Integral Equations and Applications*, 29(1):107–136, 2017.
- [21] F. Henríquez and C. Jerez-Hanckes. Multiple Traces Formulation and Semi-Implicit Scheme for Modelling Biological Cells under Electrical Stimulation. *ESAIM Mathematical Modelling and Numerical Analysis*, 52(2):659–703, 2018.
- [22] F. Henríquez, C. Jerez-Hanckes, and F. Altermatt. Boundary Integral Formulation and Semi-Implicit Scheme coupling for Modeling Cells under Electrical Stimulation. *Numerische Mathematik*, 136:101–145, 2017.
- [23] R. Hiptmair and C. Jerez-Hanckes. Multiple Traces Boundary Integral Formulation for Helmholtz Transmission Problems. *Advances in Computational Mathematics*, 37(1):39–91, 2012.
- [24] C. Jerez-Hanckes, C. Pérez-Arancibia, and C. Turc. Multitrace/singletrace formulations and Domain Decomposition Methods for the solution of Helmholtz transmission problems for bounded composite scatterers. *Journal of Computational Physics*, 350:343–360, 2017.
- [25] C. Jerez-Hanckes, J. Pinto, and S. Tournier. Local multiple traces formulation for high-frequency scattering problems. *Journal of Computational and Applied Mathematics*, 289:306–321, 2015.
- [26] C. Jerez-Hanckes, J. Pinto, and S. Tournier. Local Multiple Traces Formulation for High-Frequency Scattering Problems by Spectral Elements. In *Scientific Computing in Electrical Engineering*, pages 73–82. Springer, 2016.
- [27] M. Lopez-Fernandez and S. Sauter. Generalized Convolution Quadrature with variable time stepping. *IMA Journal of Numerical Analysis*, 33(4):1156–1175, 2013.
- [28] M. Lopez-Fernandez and S. Sauter. Generalized Convolution Quadrature based on Runge-Kutta methods. *Numerische Mathematik*, 133(4):743–779, 2016.
- [29] C. Lubich. Convolution Quadrature and Discretized Operational Calculus. I. *Numerische Mathematik*, 52(2):129–145, 1988.
- [30] C. Lubich. Convolution Quadrature and Discretized Operational Calculus. II. *Numerische Mathematik*, 52(4):413–425, 1988.

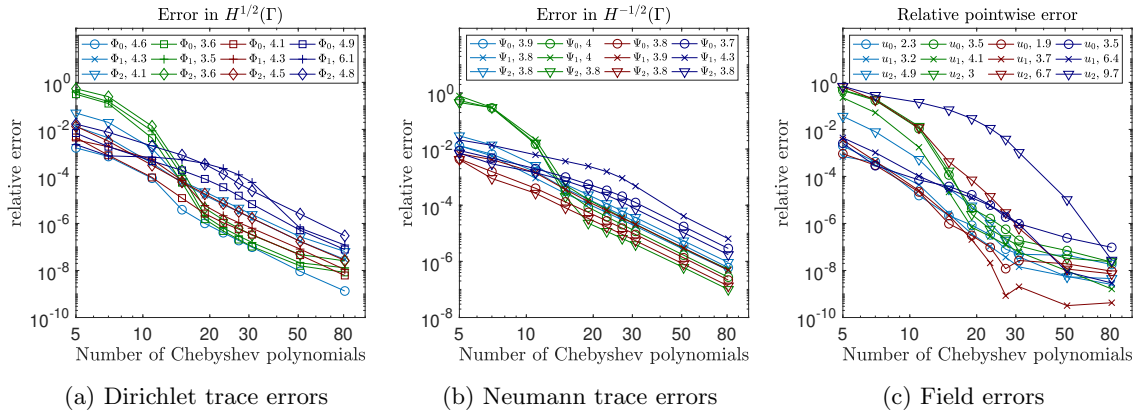
- [31] C. Lubich and A. Ostermann. Runge-Kutta Methods for Parabolic Equations and Convolution Quadrature. *Mathematics of Computation*, 60(201):105–131, 1993.
- [32] A. Pazy. *Semigroups of linear operators and applications to partial differential equations*, volume 44. Springer Science & Business Media, 2012.
- [33] T. Qiu. *Time Domain Boundary Integral Equation methods in Acoustics, Heat diffusion and Electromagnetism*. PhD thesis, University of Delaware, 2016.
- [34] T. Qiu and F.-J. Sayas. The Costabel-Stephan system of Boundary Integral Equations in the Time Domain. *Mathematics of Computation*, 85(301):2341–2364, 2016.
- [35] D.-I. A. Rieder. *Convolution Quadrature and Boundary Element Methods in wave propagation*. PhD thesis, Technische Universität Wien, 2017.
- [36] F.-J. Sayas. *Retarded Potentials and Time Domain Boundary Integral Equations: A Road Map*, volume 50. Springer, 2016.
- [37] O. Steinbach. *Numerical approximation methods for elliptic boundary value problems: finite and boundary elements*. Springer Science & Business Media, 2007.
- [38] L. N. Trefethen. *Approximation theory and approximation practice*, volume 128. Siam, 2013.
- [39] G. Wanner and E. Hairer. *Solving ordinary differential equations II*. Springer Berlin Heidelberg, 1996.
- [40] G. Wanner, E. Hairer, and S. P. Norsett. *Solving ordinary differential equations I*. Springer Berlin Heidelberg, 1993.



(a) Circle with two subdomains.

(b) Square with four subdomains.

Figure 3: Geometries used for numerical experiments.



(a) Dirichlet trace errors

(b) Neumann trace errors

(c) Field errors

Figure 4: Different relative error norms for the two subdomains case measured with respect to a highly resolved solution. Legends show estimated orders of convergence obtained by means of least squares fitting for traces and fields from subdomains $\ell = 0, 1, 2$.

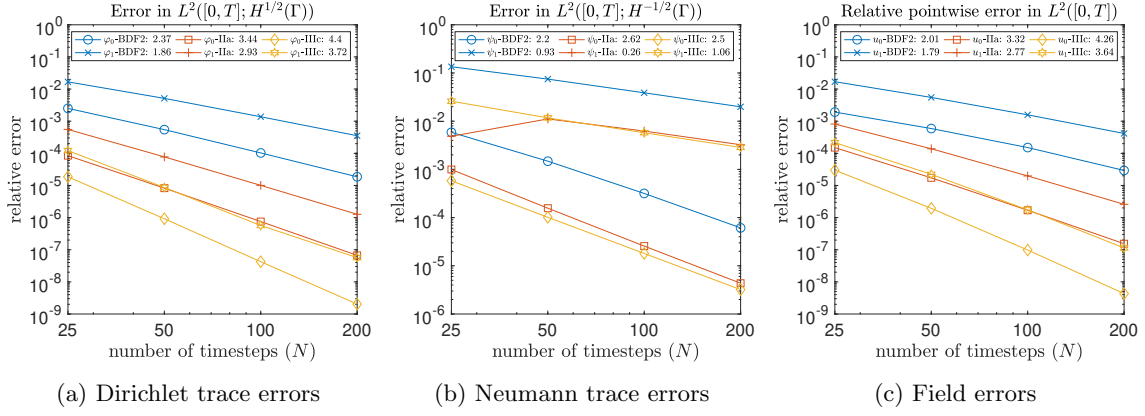


Figure 5: Relative errors for the transmission problem measured with respect to the analytical solution. Errors are computed as explained in (56) and (57). Legends show the estimated order of convergence obtained by means of least-squares fittings for traces and fields from subdomains $\ell = 0, 1$.

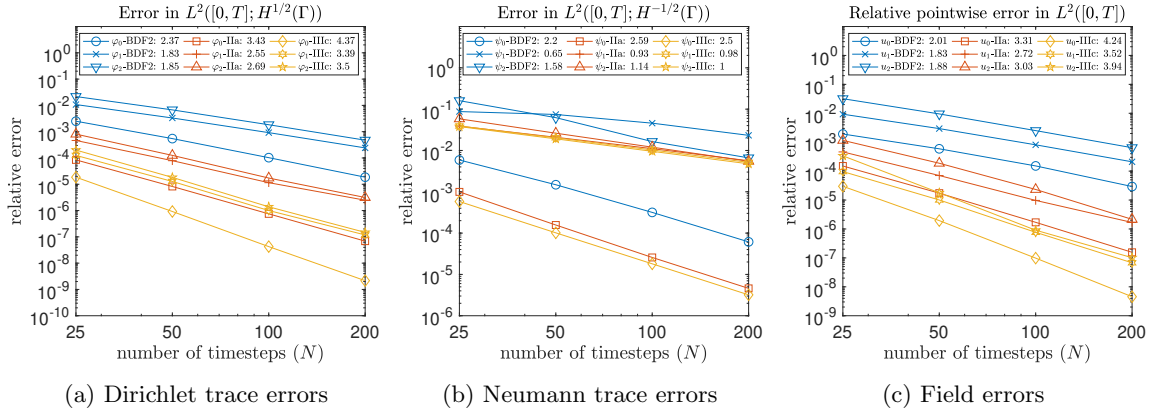


Figure 6: Relative errors for the two artificial-subdomains case measured with respect to the analytical solution. Errors are computed as explained in (56) and (57). Legends show estimated order of convergence obtained by means of least squares fitting for traces and fields from subdomains $\ell = 0, 1, 2$.

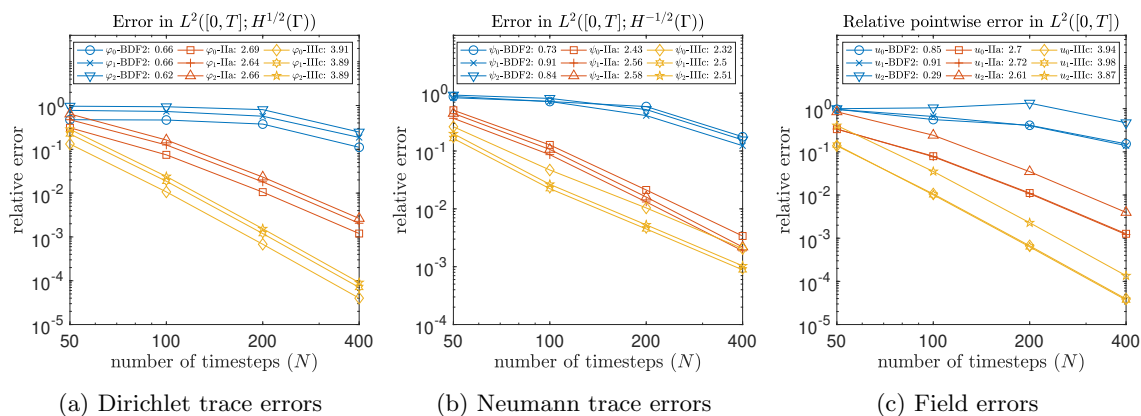


Figure 7: Relative errors for the two subdomains case measured with respect to a highly resolved solution. Errors are computed as explained in (56) and (57). Legends show methods used and estimated order of convergence obtained by means of least squares fitting for traces and fields from subdomains $\ell = 0, 1, 2$.

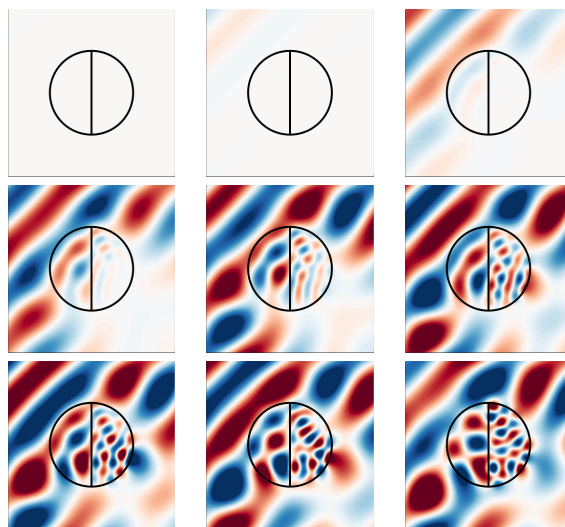


Figure 8: Snapshots of the computed field from problem in Section 6.4 for the times

$$t = 0, 1.25, 2.5, 3.75, 5, 6.25, 7.5, 8.75, 10.$$

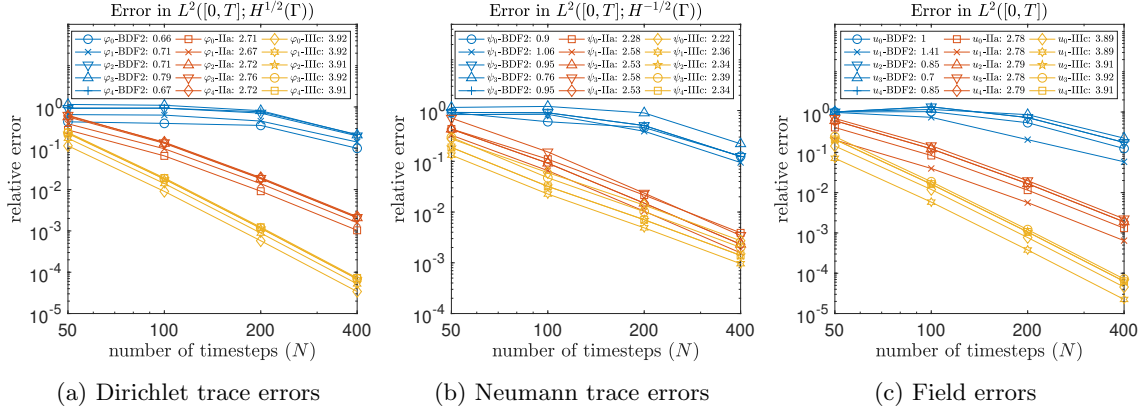


Figure 9: Relative errors for the four subdomains case measured with respect to a highly resolved solution. Errors are computed as explained in (56) and (57). Legends indicate estimated order of convergence obtained by means of least squares fitting for traces and fields from subdomains $\ell = 0, 1, 2, 3$.

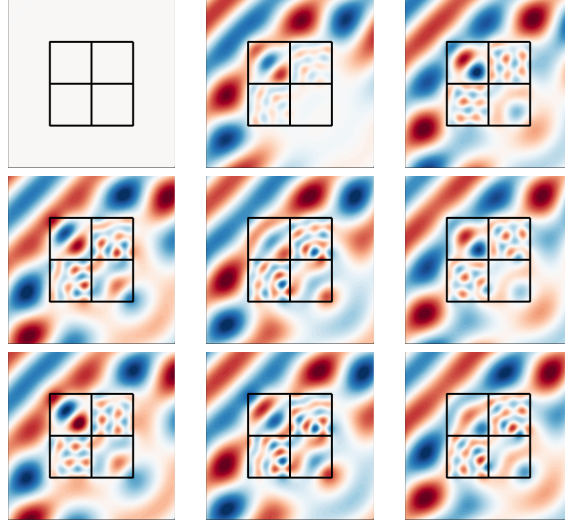


Figure 10: Snapshots of the computed field from problem in Section 6.5

$t = 0, 1.25, 2.5, 3.75, 5, 6.25, 7.5, 8.75, 10$.

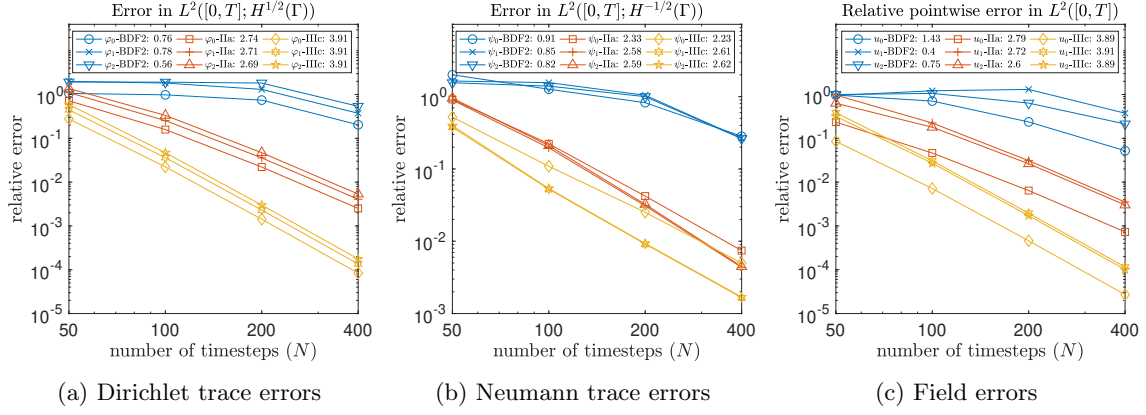


Figure 11: Relative errors for the two subdomains case in a kite-shaped domain, measured with respect to a highly resolved solution. Errors are computed as explained in (56) and (57). Legends indicate estimated order of convergence obtained by means of least squares fitting for traces and fields from subdomains $\ell = 0, 1, 2$.

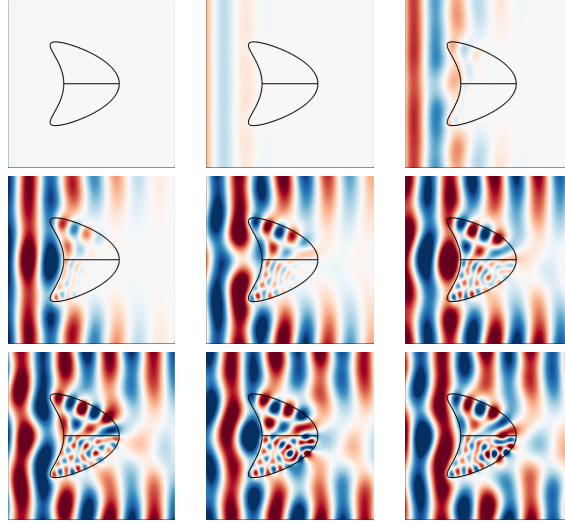


Figure 12: Snapshots of the computed field from problem in Section 6.6 for times

$$t = 0.5, 1.5, 2.5, 3.5, 4.5, 5.5, 6.5, 7.5, 8.5.$$